Visualizing Side Chains of Invisible Protein Conformers by Solution NMR

Guillaume Bouvignies[1,2,3], **Pramodh Vallurupalli**[1,2,3] **and Lewis E. Kay**[1,2,3,4]

*1 - **Department of Molecular Genetics,** The University of Toronto, Toronto, Ontario M5S 1A8, Canada*
*2 - **Department of Biochemistry,** The University of Toronto, Toronto, Ontario M5S 1A8, Canada*
*3 - **Department of Chemistry,** The University of Toronto, Toronto, Ontario M5S 1A8, Canada*
*4 - **Program in Molecular Structure and Function,** Hospital for Sick Children, 555 University Avenue, Toronto, Ontario M5S 1A8, Canada*

***Correspondence to Lewis E. Kay:** Departments of Molecular Genetics, Biochemistry and Chemistry, The University of Toronto, Toronto, Ontario M5S 1A8, Canada. kay@pound.med.utoronto.ca*
http://dx.doi.org/10.1016/j.jmb.2013.10.041
Edited by P. Wright

Abstract

Sparsely populated and transiently formed protein conformers can play key roles in many biochemical processes. Understanding the structure function paradigm requires, therefore, an atomic-resolution description of these rare states. However, they are difficult to study because they cannot be observed using standard biophysical techniques. In the past decade, NMR methods have been developed for structural studies of these elusive conformers, focusing primarily on backbone ^{1}H, ^{15}N and ^{13}C nuclei. Here we extend the methodology to include side chains by developing a ^{13}C-based chemical exchange saturation transfer experiment for the assignment of side-chain aliphatic ^{13}C chemical shifts in uniformly ^{13}C labeled proteins. A pair of applications is provided, involving the folding of β-sheet Fyn SH3 and α-helical FF domains. Over 96% and 89% of the side-chain ^{13}C chemical shifts for excited states corresponding to the unfolded conformation of the Fyn SH3 domain and a folding intermediate of the FF domain, respectively, have been obtained, providing insight into side-chain packing and dynamics.

Introduction

A major goal of structural biology is to delineate the relationship between three-dimensional structure and biological function. The main technologies that are currently exploited in this regard, including X-ray diffraction, NMR and cryo-electron microscopy, have largely focused on studies of native-state conformations of biomolecules and typically assume that the experimental data can be explained in the context of a single dominant structure. However, biomolecules such as proteins and nucleic acids are often dynamic, with their function modulated by exchange between different conformations [1,2]. Examples in the literature that illustrate the functional importance of conformational exchange include studies of protein folding [3] and misfolding [4–6], ligand binding [7,8], enzyme catalysis [9–12] and molecular recognition [2,13]. It is thus important to broaden the scope of structural biology to include both descriptions of the ground-state conformer and other conformers that exchange with it.

Solution NMR spectroscopy has emerged as an important tool for characterizing the kinetics and thermodynamics of such exchange processes along with the structures of the interconverting conformers [14–16]. Here the development of relaxation-dispersion-based approaches for studies of biomolecules has been pivotal because it is possible to obtain detailed structural information about sparsely populated, transiently formed states, so-called conformationally excited states, that cannot be observed directly in NMR spectra [14]. The first atomic-resolution structures of such conformers are now emerging [6,17–19].

To date, the great majority of studies of protein conformational exchange have made use of backbone ^{1}H, ^{15}N or ^{13}C spin probes in concert with Carr–Purcell–Meiboom–Gill (CPMG) relaxation dispersion experiments [20]. Central to the success of

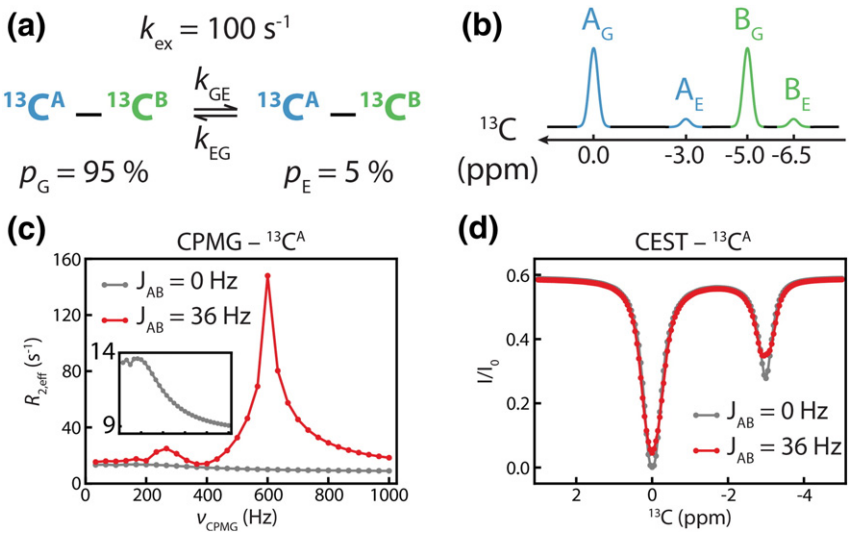

Fig. 1. Accurate ^{13}C chemical shifts can be extracted from CEST, but not from CPMG, dispersion profiles recorded on uniformly ^{13}C labeled molecules. (a) Molecular fragment comprising a two-spin ^{13}C–^{13}C scalar coupled spin system attached to a molecule that exchanges between *G* and *E* states, as indicated. (b) One-dimensional ^{13}C NMR spectrum of the fragment. Peaks derived from the excited state are typically not observed but are shown here for clarity. (c) The ^{13}C CPMG dispersion profile of carbon C^A, plotting the effective transverse relaxation rate $R_{2,eff}$ as a function of ν_{CPMG} [1/(2δ), where δ is the spacing between refocusing pulses], contains spikes that result from magnetization transfer between scalar coupled carbons, C^A and C^B (red). When J_{AB} = 0 Hz, the gray profile that reflects the chemical exchange process of interest is obtained (enlarged in the inset). The simulations were performed following a density matrix approach described in detail previously [40]. (d) ^{13}C CEST profile of C^A. The dip corresponding to the excited state of C^A is at the same position for J_{AB} = 0, 36 Hz so that the excited-state chemical shift can be accurately measured in the coupled ^{13}C–^{13}C spin system.

these methods has been the development of labeling approaches that produce isolated NMR active nuclei, eliminating magnetic interactions such as homonuclear scalar couplings that derive from adjacent spin pairs that would otherwise interfere with the extraction of accurate exchange parameters (see below). Our laboratory has, therefore, introduced isotope-labeling schemes that generate proteins with isolated $^{13}C^{\alpha}$ [21], $^{1}H^{\alpha}$ [22] or methyl ^{13}C spins [21,23], thereby side-stepping issues with ^{13}C–^{13}C or ^{1}H–^{1}H couplings. It is thus possible to obtain $^{13}C^{\alpha}$ and $^{1}H^{\alpha}$ chemical shifts of the excited state that are powerful indicators of secondary structure or to focus on larger protein systems by using methyl dispersion experiments [24].

With studies of invisible excited states focusing on backbone spin probes now reaching a mature stage, it is clear that further applications must extend to side chains. Side-chain interactions are critical for protein stability, for function and for molecular recognition [25], and a first step in studying such interactions by NMR involves obtaining chemical shift assignments. However, these are difficult to measure in the excited state, in particular, when carbon is concerned. Attempts to produce proteins with isolated $^{13}C^{\beta}$ spins have proven to be only moderately successful [26]. Although proteins with alternate ^{13}C–^{12}C labeling can be prepared at many sites [27], this requires protein production using special bacterial strains, two different samples for coverage of the majority of ^{13}C positions, and results in incomplete labeling that ultimately decreases signal to noise. Samples produced with random fractional labeling are also not optimal from a sensitivity standpoint and there is an issue that a sizable percentage of adjacent carbons are ^{13}C labeled. From a sensitivity perspective, the best approach is one that makes use of uniformly ^{13}C labeled samples that can be prepared with relative ease and that are almost always produced at the start of any NMR project. However, such samples re-introduce scalar coupling interactions that are detrimental to the performance of the CPMG dispersion experiment [28].

Here we describe a method for probing exchange at carbon side-chain positions in proteins based on chemical exchange saturation transfer (CEST) that is insensitive to the presence of ^{13}C–^{13}C couplings. The utility of saturation transfer to study chemical exchange processes in molecules dates to the pioneering studies of Forsen and Hoffman in the early 1960s [29], with subsequent applications to protein systems in the 1970s [30,31]. The methodology has also been exploited in the magnetic resonance imaging field by making use of the fact that weak metabolite signals can be amplified many fold in a process involving exchange of protons with water that leads to transfer of saturation to the very concentrated water signal [32,33]. Recently, these

ideas have been extended to studies of sparsely populated, transiently formed protein states, focusing on backbone ^{15}N [34,35], ^{13}C [36–38] and ^{1}H [39] spins using weak continuous wave, radiofrequency fields. We show that they can be further extended to measure excited-state ^{13}C chemical shifts at *every* aliphatic side-chain position in a uniformly ^{13}C labeled protein, without the complications that would prevent such measurements by "standard" CPMG relaxation-dispersion-based experiments. The methodology thus significantly extends our ability to bring invisible protein states into focus.

Results

Figure 1 illustrates the power of the CEST approach in studies of protein systems that are uniformly ^{13}C labeled in relation to the more established CPMG method. Consider an isolated ^{13}C–^{13}C spin pair, with J_{AB} = 36 Hz, that is part of a molecule that exchanges between ground (G) and excited (E) states (Fig. 1a) with an exchange rate of $k_{ex} = k_{GE} + k_{EG} = 100\ s^{-1}$ and where the fractional population of G (p_G = 0.95) is much larger than $p_E = 1 - p_G$ so that only the ground-state peaks can be observed in spectra. Note that, in Fig. 1b, the intensities of the E state peaks have been scaled up for the purposes of illustration. In a typical CPMG experiment, the effective decay rates of transverse magnetization ($R_{2,eff}$, proportional to the linewidth) derived from ground-state peaks are measured as a function of a train of chemical shift refocusing pulses that are applied during a fixed delay period [14,41]. Focusing on the ground-state peak from C^A (chemical shift of 0 ppm; Fig. 1b), we obtain a dispersion profile, $R_{2,eff}$ *versus* the inverse of the pulse spacing (ν_{CPMG}), as shown in Fig. 1c (red). Notably, $R_{2,eff}(\nu_{CPMG})$ becomes large for ν_{CPMG} values of ~300 Hz and then much larger for ν_{CPMG} = 600 Hz. This reflects a Hartmann–Hahn transfer [42] of magnetization from C^A to C^B that is a function of the chemical shift difference between the two coupled carbons and the number of pulses applied and is unrelated to the chemical exchange process of interest. It significantly complicates the extraction of accurate exchange parameters and excited-state chemical shifts, especially when more complex spin systems are considered such as those in amino acids. In contrast, when the scalar coupling is "turned off", J_{AB} = 0 Hz, a very different profile is obtained, one that decreases smoothly as the number of refocusing pulses (ν_{CPMG}) increases (gray). This second dispersion profile reports only on chemical exchange ($G \rightleftharpoons E$) and not on the magnetization exchange process that occurs via evolution due to scalar couplings ($A \rightleftharpoons B$) and can be readily fit to extract the exchange parameters of interest.

A very different scenario is observed when using the CEST experiment (Fig. 1d). Here the starting point is z-magnetization. A weak continuous wave, radiofrequency field (B_1 field), typically 10–50 Hz, is applied for a duration T_{CEST} over the range of ^{13}C frequencies (one at a time) that is relevant for the molecule studied. At each position of the weak B_1 field the intensities of magnetization of all carbons in the molecule, C^A is shown in the present example, are measured after the T_{CEST} duration (I) and plotted as I/I_o *versus* position of the B_1 field, where I_o is the intensity in the absence of the CEST element. A major dip in intensity is observed when the radiofrequency is placed at the resonance position of the ground state (0 ppm) since the magnetization becomes saturated. A second dip is also observed when the radiofrequency is proximal to the resonance frequency of the excited state (−3 ppm) since perturbation of magnetization of C^A in state E is transferred to the corresponding position in G via chemical exchange (Fig. 1d). It is worth emphasizing that only longitudinal magnetization from the (visible) ground state is measured. The signal from the (invisible) excited state becomes amplified by the chemical exchange process that connects G with E, by the fact that long exchange delays, T_{CEST}, can be used and of course by the fact that it is measured indirectly by quantifying the ground-state intensity. Notably, very similar spectra are observed for J_{AB} = 0, 36 Hz, and the excited-state dip is at an identical position in both cases so that accurate measures of carbon chemical shifts can be obtained using the CEST approach, even in a ^{13}C scalar coupled spin system.

Applications to complex molecules such as proteins are challenged by the need to resolve as many correlations as possible. Here we have used a two-dimensional (2D) NMR experiment (see Supplementary Fig. 1 and Supplementary Table 1), with the magnetization transfer scheme described succinctly as $^{1}H \rightarrow {}^{13}C(t_1) \rightarrow CEST \rightarrow {}^{1}H(t_2)$. Magnetization is transferred from ^{1}H to ^{13}C and chemical shift recorded during t_1. Subsequently, ^{13}C magnetization is restored to the z-axis and a weak B_1 field applied for a time T_{CEST} during the CEST interval that immediately precedes a transfer period back to ^{1}H for detection.

As a first demonstration of the methodology, for which cross-validation is especially straightforward, we consider an application to the G48A Fyn SH3 domain, a small 60-residue module that plays an important role in protein recognition involved in a range of signaling events [43]. It has previously been shown by stopped-flow fluorescence measurements and CPMG relaxation dispersion experiments [44] that this module interconverts on the millisecond timescale between a long-lived, highly populated native state and a transiently formed, sparsely populated unfolded conformer. ^{15}N CEST experiments recorded at 25 °C

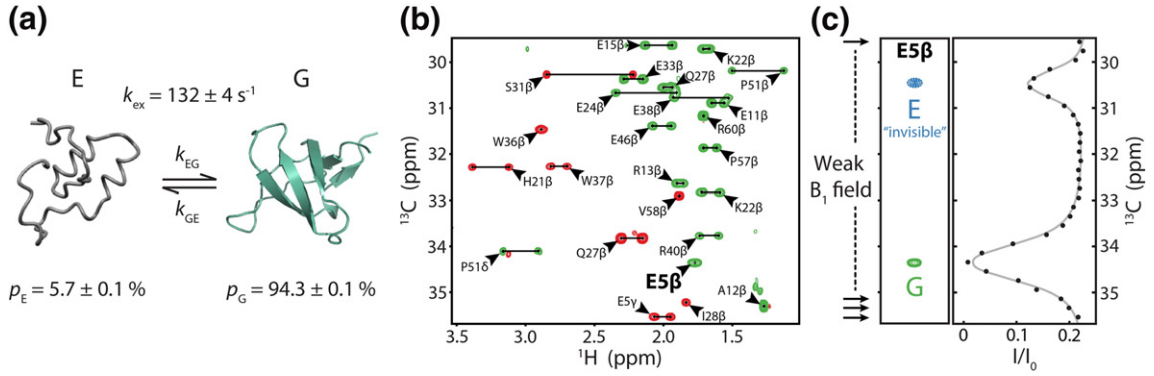

Fig. 2. An application of ^{13}C CEST to the G48A Fyn SH3 domain. (a) The protein exchanges between populated native and sparsely populated unfolded states, k_{ex} = 132 s^{-1}, 25 °C. (b) Portion of the ^{13}C–^{1}H correlation map recorded with the pulse scheme of Supplementary Fig. 1a (CT-t_1), T_{CEST} = 0, 14.0 T, 25 °C. Cross-peaks in red and green have opposite phase (sign) that depends on the number of directly bonded ^{13}C coupling partners and whether the correlation is aliased an even or odd number of times. Pairs of correlations separated by horizontal lines are derived from non-equivalent protons of the same methylene group. Only the folded state correlations are observed in spectra, but dips at the positions of the excited-state resonances can be clearly seen in CEST profiles, shown here for E5β, T_{CEST} = 0.25 s, B_1 = 23 Hz (c).

establish that k_{ex} = 132 ± 4 s^{-1}, with p_E = 5.7 ± 0.1% (Fig. 2a). Figure 2b plots a region from the ^{13}C–^{1}H correlation map measured with the scheme of Supplementary Fig. 1a with T_{CEST} = 0, 25 °C and 14.0 T, and the intensity of the correlation from E5β is displayed as a function of the position of the CEST radiofrequency field (23 Hz) in Fig. 2c. The chemical shift of the excited-state C$^{\beta}$ carbon from E5 is immediately apparent from the trace.

We have recorded a series of ^{13}C CEST experiments, as discussed in Materials and Methods and Supplementary Information, so that all of the aliphatic ^{13}C chemical shifts of the excited state could be obtained. Figure 3 shows CEST profiles for each ^{13}C carbon of L18 (a), K25 (b) and I28 (c) along with $\Delta\varpi = \varpi_E^j - \varpi_G^j$, where ϖ_K^j is the chemical shift of carbon j in state K ($K \in \{G,E\}$); all of the available profiles are shown in Supplementary Fig. 2, with chemical shifts summarized in Supplementary Table 2 and deposited in the Biological Magnetic Resonance Data Bank (BMRB) (accession number 19590). Chemical shifts, linewidths and exchange parameters are fit using a procedure described in Materials and Methods, with the shift of the ground-state carbon that is measured from a separate ^{13}C–^{1}H correlation map input as a fixed parameter. In addition to the dip from the ground state, a smaller dip is observed from the excited state for many of the carbons, but not all since $\Delta\varpi \sim 0$ in

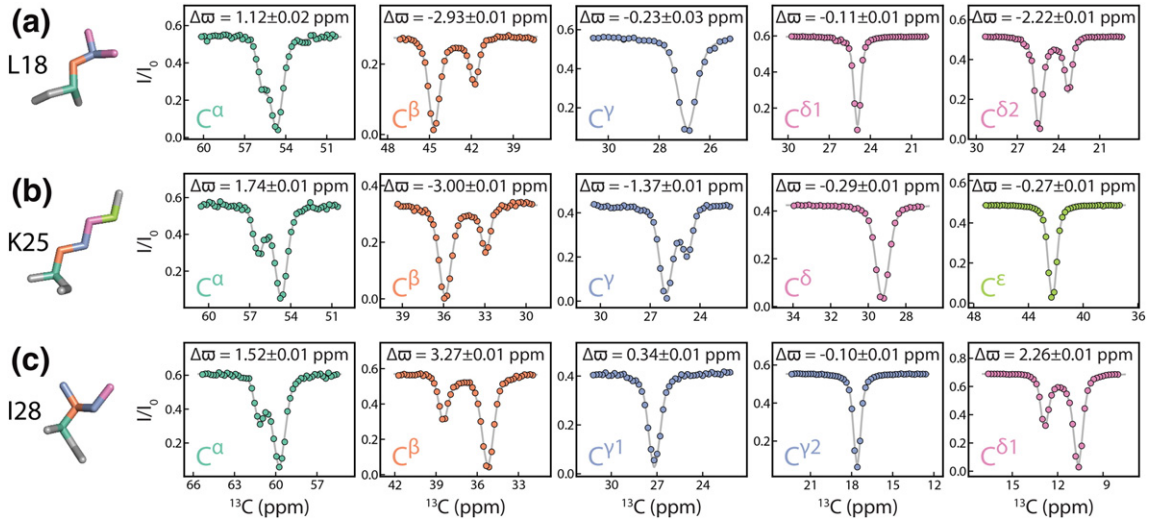

Fig. 3. Measuring ^{13}C side-chain chemical shifts of excited protein states. CEST profiles for each ^{13}C carbon of L18 (a), K25 (b) and I28 (c) from the G48A Fyn SH3 domain, 25 °C, along with the difference in chemical shifts between corresponding nuclei in ground and excited states, Δϖ. Errors are calculated on the basis of a covariance matrix method [45].

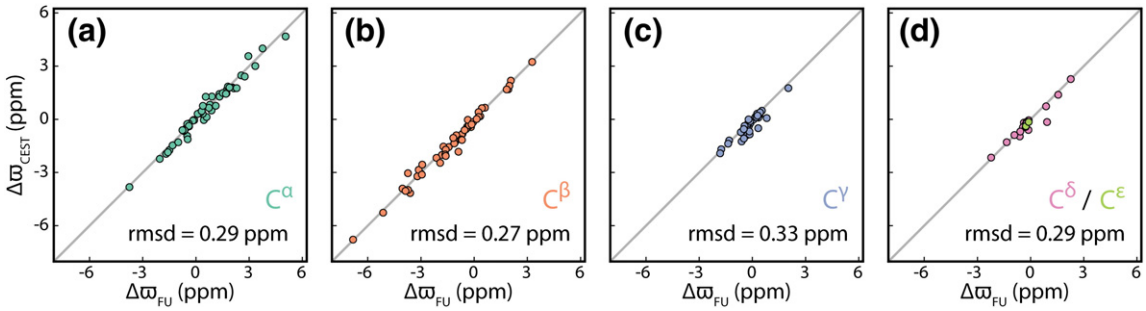

Fig. 4. Accurate aliphatic ^{13}C chemical shifts are obtained. Linear correlation plots of $\Delta\varpi$ values measured from ^{13}C CEST ($\Delta\varpi_{CEST}$) and computed assuming that the unfolded state chemical shifts are well approximated by random-coil values ($\Delta\varpi_{FU}$) are shown for (a) C^{α}, (b) C^{β}, (c) C^{γ} and (d) C^{δ}, C^{ε} carbons of the G48A Fyn SH3 domain, 25 °C. The rmsd values between $\Delta\varpi_{CEST}$ and $\Delta\varpi_{FU}$ values are listed. Random-coil C^{α}/C^{β} values are from Tamiola *et al.* [46], with the remaining carbons from Wishart *et al.* [47].

some cases. Notably, multiplet fine structure due to ^{13}C–^{13}C couplings is not seen in the CEST profiles. As discussed previously, the dips are artificially broadened by the B_1 field [35]; for fields on the order of 10–15 Hz, multiplet components begin to emerge, but not for values on the order of 25 Hz used here. Observed linewidths therefore depend on intrinsic relaxation rates and exchange lifetimes, the number of directly coupled ^{13}C partners, the size of the radio-frequency field used and contributions from exchange involving processes connecting additional states to *G* and *E* [35] (and that are not included in the model used). All of the data for the G48A Fyn SH3 domain could be well fit to a two-site exchange model, taking into account coupling partners and assuming values of 35 Hz and 51 Hz for aliphatic–aliphatic and aliphatic–carbonyl or aliphatic–aromatic ^{13}C–^{13}C couplings, respectively (see Materials and Methods).

Supplementary Figure 3a shows a bar graph illustrating the completeness of the data. Out of 171 aliphatic carbon sites, we have obtained excited-state ^{13}C chemical shifts for 164 positions. A number of $^{13}C^{\alpha}$ shifts could not be measured (5 of 60) due to the proximity of the corresponding $^{1}H^{\alpha}$ shift to water (a single 90% H_2O sample was used in all measurements). Certainly, very near if not complete assignments of $^{13}C^{\alpha}$ shifts would be obtained using a D_2O sample. As a means of cross-validation of the measured shifts, we have compared $\Delta\varpi$ values obtained from fits of the CEST profiles with calculated values assuming that the excited-state chemical shifts are given by tabulated random-coil values (Fig. 4). The agreement is excellent and the rmsd between experiment and predicted values, less than 0.35 ppm, is an upper bound for the errors in experimental measurements.

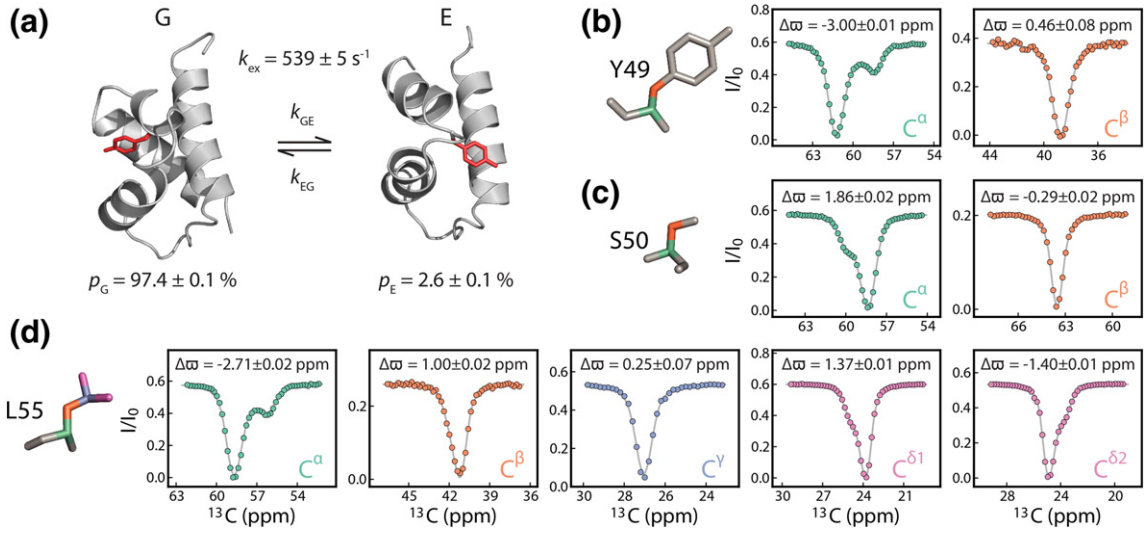

Fig. 5. An application of ^{13}C CEST to the L24A FF domain. (a) The protein exchanges between a populated native state and a conformer that corresponds to an on-pathway folding intermediate [48], k_{ex} = 539 s^{-1}, 25 °C. The excited-state conformer adopts an alternative folded structure that places Y49 (red) into a cavity that is formed by the replacement of Leu with Ala at position 24. (b–d) Selected ^{13}C CEST profiles for Y49 (b), S50 (c) and L55 (d), along with extracted $\Delta\varpi$ values.

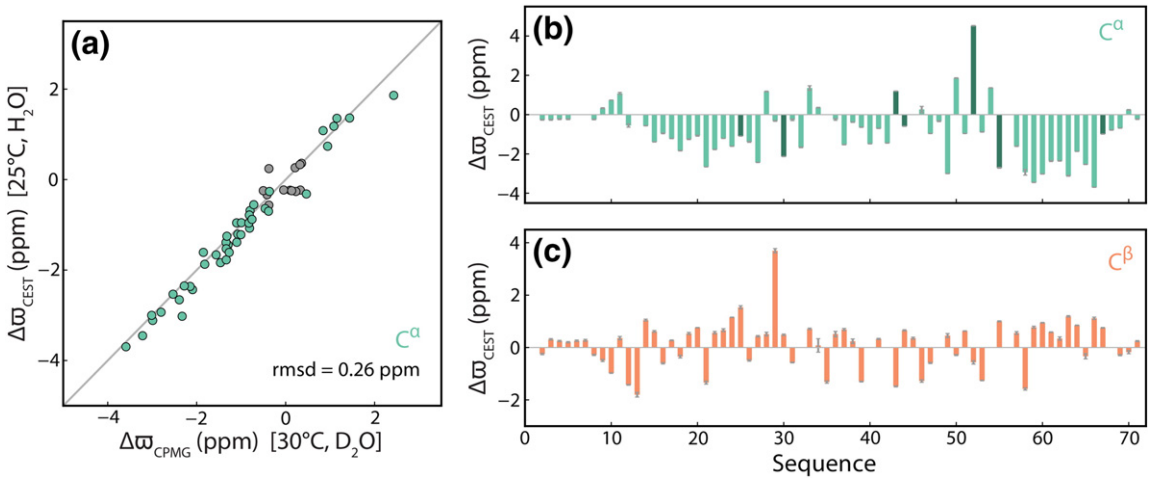

Fig. 6. Validation of L24A FF domain $^{13}C^\alpha$ chemical shifts. (a) Linear correlation plot comparing $^{13}C^\alpha$ $\Delta\varpi$ values obtained from CEST ($\Delta\varpi_{CEST}$) with shift differences extracted from fits of CPMG data sets ($\Delta\varpi_{CPMG}$) from a previous study [48]. Circles in gray denote those residues for which the sign of $\Delta\varpi_{CPMG}$ could not be obtained experimentally. (b and c) Bar graphs of $^{13}C^\alpha$ (b) and $^{13}C^\beta$ (c) $\Delta\varpi$ values, extracted from CEST profiles as described in the text. Positions denoted in dark green are those for which $^{13}C^\alpha$ shift differences cannot be obtained by CPMG relaxation dispersion (I,L,V) due to the labeling scheme used [21].

The Fyn SH3 system described above is particularly favorable for CEST because of the relatively high population of the excited state (5.7%) and the slow exchange rate (130 s^{-1}) that does not introduce excessive broadening of excited-state peaks. In contrast, CPMG relaxation dispersion studies would be challenged by this slow exchange timescale, leading to a partial correlation of k_{ex} and p_E. As a further test of the methodology, we next studied the L24A FF domain (see below) that exchanges between the native state and an on-pathway folding intermediate with a well-defined structure, albeit somewhat different from the native form (Fig. 5a). The structure of the intermediate was previously established through an analysis of backbone ^1H, ^{15}N and ^{13}C CPMG relaxation dispersion profiles [48], but it did not include side-chain data. Notably, the L24A mutation creates a cavity in the protein that is filled by Y49 in the intermediate, but not in the native conformation. Side-chain rearrangements are thus critically important for stabilizing the intermediate, and we have measured ^{13}C chemical shifts as a first step toward a detailed characterization of side-chain structure and dynamics.

Figure 5b–d highlights CEST profiles for a number of residues, including Y49 (a) and S50 (b), that play important roles in the intermediate structure (all of the profiles are illustrated in Supplementary Fig. 4 and chemical shifts are tabulated in Supplementary Table 3 and deposited in the BMRB, accession number 19591). Notably, CEST profiles are significantly broader for the FF domain than for the SH3 domain that reflects the increased exchange rate (540 s^{-1} *versus* 132 s^{-1}, 25 °C) (Supplementary Fig. 5). In addition, the excited state is significantly less populated than for the SH3 domain (2.6% *versus* 5.7%). Because of the increased k_{ex} and lower p_E, the FF domain is a more challenging example than the SH3 module; yet, accurate chemical shifts are still obtained. As a means of cross-validation, we have compared the extracted $^{13}C^\alpha$ $\Delta\varpi$ values from CPMG- and CEST-based methods (Fig. 6a), and the agreement is excellent (0.3 ppm rmsd). Furthermore, the CEST approach has the added benefit in that all $^{13}C^\alpha$ shift values can be obtained, while the scheme used to produce "isolated" $^{13}C^\alpha$ spins that is required for the CPMG measurements does not label (Leu) or generate isolated spins (Ile, Val) at the desired C^α position [21]. Measured $^{13}C^\alpha$ and $^{13}C^\beta$ $\Delta\varpi$ values from the CEST approach are plotted as a function of residue position in Fig. 6b and c, respectively, with shift differences obtained for over 90% of the residues. Interestingly, a large change in $\Delta\varpi$ is observed for the C^β nucleus of R29, $\Delta\varpi$ = 3.7 ppm, that is similar to the predicted value of 4.5 ppm that would accompany a transition to an unfolded conformation. The remaining C^α/C^β $\Delta\varpi$ values in this region are all consistent with an "unfolded-like" conformation, suggesting that the loop connecting helices 1 and 2 in the rare state is less well defined than for the native conformation. Indeed, estimated order parameters based on chemical shifts [49] indicate that the loop is more flexible in the excited state than in the natively formed structure [48]. The level of completeness of the side-chain assignments for the sparsely populated FF domain folding intermediate is shown as a function of side-chain carbon in Supplementary Fig. 3b. Overall, 90% of the carbons have been assigned.

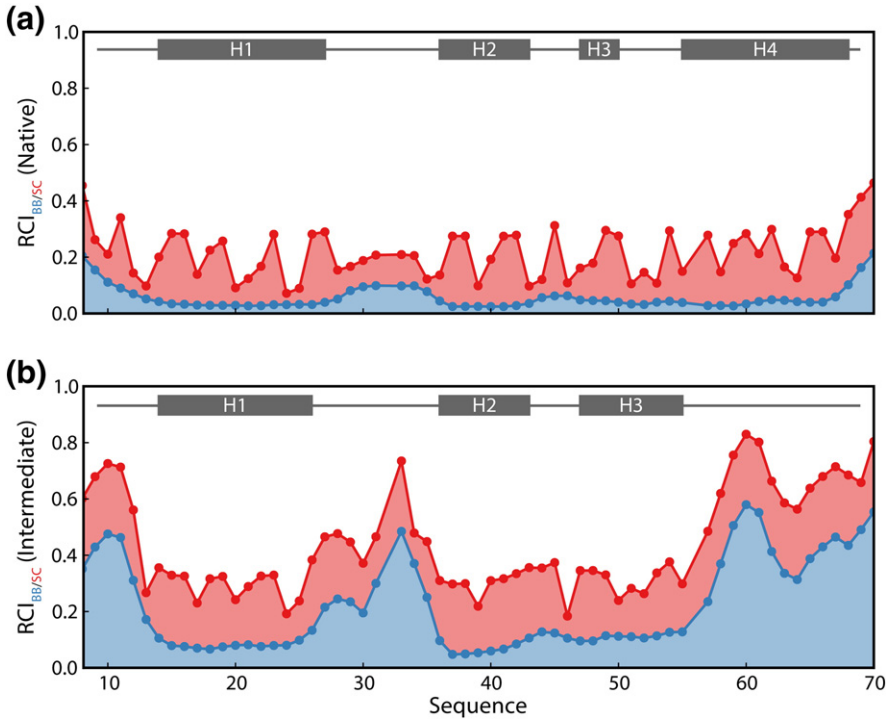

Fig. 7. Side-chain mobility from ^{13}C chemical shifts. RCI plots [49,56] for the native (a) and intermediate (b) states of the L24A FF domain as a function of residue number. The first nine residues are omitted as they are completely flexible. RCI_{BB} and RCI_{SC} values are shown in blue and red, respectively, along with the secondary structural elements in each of the states. Large RCI values are indicative of increased mobility, with the rmsd of a given side chain obtained from molecular dynamics simulations estimated from the relation rmsd = $RCI_{SC} \times 9$ Å [56].

Discussion

We have presented a simple ^{13}C CEST experiment for measuring aliphatic side-chain chemical shifts of "invisible" excited conformational states of proteins. As a first example, an application to the G48A Fyn SH3 domain has been described where 96% of the side-chain carbon assignments were obtained. This value compares favorably with what is typically reported for ground-state conformers. We see no evidence for any residual native-like secondary structure in the excited state on the basis of $^{13}C^{\alpha}$ and $^{13}C^{\beta}$ chemical shifts that are very sensitive indicators of such. Moreover, the close similarity between measured ^{13}C shifts past C^{β} and predicted values based on random-coil polypeptides argues against long-lived tertiary interactions in the G48A Fyn SH3 unfolded state as well. Furthermore, in support of these results, fits of ^{15}N CEST profiles (data not shown) did not improve when a parameter was included in the analysis to take into account exchange between the unfolded state and additional conformers.

It is interesting that folding intermediates have been observed for G48M and G48V Fyn SH3 domains [3], but not for the G48A module studied here. It may be that the longer side chain at position 48 for G48M and G48V, relative to G48A, facilitates the formation of interactions in the intermediate that help stabilize it to the point where its population is sufficient to be observed by either CEST or CPMG methods (more than ~0.5%). In a similar regard, the approximately 5-fold slower folding rate of G48A relative to G48M and G48V has been explained by the fact that Ala forms fewer stabilizing contacts in the folding transition state than either of the longer side chains of Met or Val [44].

We have also considered a second example, involving an L24A mutant of the FF domain that exchanges between the native state and a well-defined folding intermediate (k_{ex} = 540 s^{-1}, 25 °C). This intermediate has been shown previously by both stopped-flow fluorescence [50] and CPMG experiments [17,51] to be on the folding pathway. Both studies point to a fast collapse from the unfolded ensemble to the intermediate (rates on the order of tens of thousands per second) that is then followed by a relatively slow folding step to the native structure. The intermediate thus functions as a kinetic trap, slowing the overall folding rate, as has been observed in studies of the folding of other helix bundle proteins [52–55]. Figure 5a shows the structures of both native and intermediate states of the L24A FF domain. The intermediate structure is,

in general, well formed and can be described as an alternative fold of the FF domain. Indeed, it is the stability of this intermediate state that slows the overall folding. Notably, there are significant differences in side-chain packing between intermediate and native states, as highlighted by the position of Tyr49 (red in Fig. 5a) that inserts into a cavity that is created by the L24A mutation [48]. Aliphatic ^{13}C side-chain assignments provide an avenue for studying packing/dynamics in the intermediate state and with the increasing development of bioinformatic methods such as side-chain chemical shift information that can be used at an initial stage of the analysis. Here we have used a recently developed approach by Berjanskii and Wishart that exploits side-chain ^{13}C chemical shifts in the calculation of RCI_{SC} parameters [56] that have been shown to be well correlated with side-chain rmsd values obtained from molecular dynamics simulations ($rmsd_{SC} = RCI_{SC} \times 9$ Å). The methodology is essentially an extension of the backbone RCI approach (RCI_{BB}), also introduced by the laboratory of Wishart [49], for estimation of protein backbone mobility. Figure 7 compares RCI_{BB} (blue) and RCI_{SC} (red) values for the native (a) and intermediate (b) states of the L24A FF domain. The first nine residues of the domain have been omitted from the plot, as these are part of a highly disordered region. As expected, in general, the RCI values for the native state are smaller than those for the intermediate, consistent with increased motional amplitudes in the intermediate conformer. This is particularly the case for the loop between helices 1 and 2 of the FF domain and for the C-terminal region, where helix 4 is well formed in the native structure, but not in the intermediate. The discrepancy is smallest for the RCI values that include helices 1, 2 and 3, which are well ordered in the excited state. Moreover, differences between RCI_{BB} and RCI_{SC} are somewhat larger for the intermediate than for the native state (red shading in Fig. 7), consistent with a less well packed intermediate structure.

As with other CEST applications that have been reported previously [35], the methodology described here works best for systems with exchange rates that fall roughly into the range 20–50 $s^{-1} < k_{ex} < 500\ s^{-1}$. We have explored the sensitivity of the CEST methodology to the exchange rate more fully through simulations, described in Supplementary Information. As k_{ex} increases past ~400 s^{-1}, the excited-state dips broaden considerably and this can lead to larger errors in the quantitation of exchange parameters, p_E and k_{ex}, although $\Delta\varpi$ values appear to be quite robust (Supplementary Fig. 6). We have also explored this question experimentally through studies of the L24A FF domain. Although the exchange rate is relatively high for CEST (k_{ex} = 540 s^{-1}, 25 °C), accurate values of chemical shifts are still readily obtained (Fig. 6), even in the case where $\Delta\varpi$ values are small. This is in keeping with the results from simulations (Supplementary Fig. 6). The exchange kinetics of the L24A FF domain make it well suited for study by CPMG approaches, and we have used such methods to characterize this system previously [21]. However, CEST offers several advantages. First, signs of chemical shift differences are immediately available from an analysis of the data (and often by inspection of the CEST profiles), without the requirement of recording additional experiments. Second, a more complete set of $^{13}C^{\alpha}$ shifts for the excited state can be obtained because uniform ^{13}C labeling is employed. Third, the very weak and, therefore, selective B_1 field of the CEST experiment means that experiments can be recorded without pathologic interference from homonuclear scalar couplings, thereby enabling measurement of excited-state side-chain ^{13}C chemical shifts.

In cases where exchange rates are outside the optimal CEST range, it may be possible to manipulate sample conditions to generate interconversion rates that are more suitable for CEST. Furthermore, the experiment will benefit from higher static magnetic fields that lead to increases in resolution in 2D ^{13}C–^{1}H correlation maps and in CEST profiles and result in longer ^{13}C T_1 values that will improve sensitivity. The ability to obtain site-specific aliphatic side-chain chemical shifts is an important step forward in characterizing protein excited states and in elucidating how they function at an atomic level.

Materials and Methods

Protein expression and purification

The gene for expression of the G48A *Gallus gallus* Fyn SH3 domain was optimized for protein production (GenScript, Piscataway, NJ, USA) and placed in a pET-29b plasmid carrying an NH_2-terminal hexa-histidine tag followed by a tobacco etch virus protease cleavage site. Uniformly $^{13}C/^{15}N$ enriched G48A Fyn SH3 domain was expressed in *Escherichia coli* BL21(DE3) cells grown in M9 minimal media (H_2O) with [$^{13}C_6$]glucose (3 g/L) and ^{15}N ammonium chloride (NH_4Cl; 1 g/L) as the unique carbon and nitrogen sources, respectively. *E. coli* BL21(DE3) cells were transformed with the plasmid and were grown in 1 L of media at 37 °C until an OD_{600} of ~0.9 was reached. Protein expression was then induced with 1 mM IPTG for 4 h. The cells were harvested by centrifugation and frozen. The protein was purified from the cells as described earlier [44,57]. A uniformly $^{13}C/^{15}N$ enriched sample of the L24A FF domain was produced as described previously by Jemth *et al.* [58].

NMR samples

An NMR sample of the G48A Fyn SH3 domain was prepared at a concentration of 2 mM U-[^{15}N,^{13}C], 0.2 mM ethylenediaminetetraacetic acid, 0.05% NaN_3 and 50 mM

sodium phosphate (pH 7.0), in 90% H_2O/10% D_2O. A second sample of the L24A FF domain was 2 mM in U-[^{15}N,^{13}C]protein, 50 mM sodium acetate, 100 mM NaCl and 90% H_2O/10% ^2H_2O (pH 5.7).

Ground-state assignment experiments

Backbone $^1H/^{13}C/^{15}N$ and side-chain aliphatic ^{13}C assignments for both G48A Fyn SH3 and L24A FF domains were obtained using standard triple resonance experiments [59] recorded at 25 °C, 11.7 T, using a spectrometer equipped with a room temperature probe. We assigned 100% (98%) of the ground-state aliphatic carbon resonances for the SH3 domain (FF domain).

CEST experiments

In order to estimate the population of the minor states for both SH3 and FF domains and the exchange rates, ^{15}N CEST experiments [35] were run at 25 °C, 11.7 T (room temperature probe), using an ^{15}N B_1 radiofrequency field strength of 27 Hz (SH3) or 28 Hz (FF), T_{CEST} = 0.5 s and 0.3 s for SH3 and FF, respectively. Nitrogen CEST methods are preferred for estimating exchange parameters because of the high sensitivity of the experiment and the smaller influence from ^{13}C couplings relative to ^{13}C CEST approaches. In the case of the SH3 domain, 61 2D planes were obtained with the position of the ^{15}N B_1 field ranging from 104.0 to 133.6 ppm in steps of 25 Hz. Each 2D data set was recorded with acquisition times ($t_{1,max}$, $t_{2,max}$) = (54.9 ms, 64.0 ms), 4 transients per free induction decay (FID) and an inter-scan delay of 1.5 s, corresponding to a net acquisition time of about 11.5 min per plane and 12 h for the complete series (data not shown). Very similar experimental parameters were used for the FF domain.

Assignment of the excited-state aliphatic ^{13}C resonances was achieved by analysis of a set of 2D aliphatic ^{13}C CEST experiments (see Supplementary Fig. 1a and b and Supplementary Table 1) that were measured at 25 °C, 14.0 T (cryogenically cooled probe), using a single ^{13}C B_1 radiofrequency field strength of 23.4 Hz (SH3) and 26.3 Hz (FF) applied for the duration T_{CEST} = 0.25 s (SH3) and 0.3 s (FF). Each 2D plane was recorded with a ^{13}C B_1 field offset increment of 30 Hz, an indirect dimension spectral width of 2.4 kHz, a direct acquisition time of $t_{2,max}$ = 64.0 ms, 4 scans per FID and a repetition delay of 1.5 s. Further experimental details are summarized in Supplementary Table 1. Optimal choice of the B_1 field depends, in general, on the exchange rate, the range of $\Delta\varpi$ values and the value of T_{CEST} chosen. As the exchange rate decreases, a larger B_1 is often preferred to increase the size of the dips derived from the excited state. By contrast, for a small range of shift differences, a smaller B_1 value is preferred since there is less broadening of the dips in the CEST profile and hence better resolution between the dips derived from major and minor states. As illustrated here, where similar B_1 fields and T_{CEST} values were used in experiments on exchanging systems with substantially different k_{ex} rates, the extraction of accurate shift differences in the CEST experiment is rather tolerant to experimental settings and values of B_1 = 20–30 Hz appear to be a good compromise for many systems.

For a robust estimate of the longitudinal relaxation rate of ground-state nuclei, each CEST data set includes a plane recorded with T_{CEST} = 0. Calibration of the weak B_1 field applied during the T_{CEST} interval was achieved by monitoring a single, on-resonance signal as a function of T_{CEST}, according to the procedure of Guenneugues *et al.* [60]. In order to limit potential errors in the calibration that could arise from evolution due to scalar couplings with adjacent ^{13}C spins, we calibrated the B_1 field at a field strength of about 200 Hz. The estimated strength of the lower B_1 field used in the CEST experiment was then obtained assuming amplifier linearity within the regime of interest.

It is worth noting that the ^{13}C decoupling that is applied during the t_1 evolution period in some of the ^{13}C CEST experiments (see Supplementary Table 1) can introduce Bloch-Siegert shifts [61]. ^{13}C shifts of the ground state that were used as fixed parameters in fits of the ^{13}C CEST profiles were thus obtained from a separate ^{13}C–^1H correlation map recorded using the pulse sequence described in Supplementary Fig. 1c. In this scheme, refocusing of the scalar coupled evolution involving aliphatic ^{13}C–aromatic/carbonyl ^{13}C spins is achieved using aromatic/carbonyl selective 180° pulses. A data set was recorded at 14.0 T (cryogenically cooled probe), 25 °C, with an indirect spectral width of 10.5 kHz, acquisition times of ($t_{1,max}$, $t_{2,max}$) = (27.8 ms, 64.0 ms), 4 transients per FID and an inter-scan delay of 1.5 s, corresponding to a net acquisition time of about 2.5 h.

Data processing

All spectra were processed and analyzed using the NMRPipe suite of programs [62]. Peak intensities, I, were quantified using the line-shape-fitting module of the package with subsequent visualization of spectra and peak picking achieved with the program Sparky [63]. Assignment of the triple resonance experiments was performed with the CCPN NMR analysis program [64].

Data analysis

All CEST intensity profiles were numerically fit using an in-house-written python program, ChemEx (available upon request), with the best-fit model parameters extracted by minimizing the standard χ^2 function

$$\chi^2(\xi) = \sum_i \left(\frac{I_i^{exp} - I_i^{calc}(\xi)}{\sigma_i^{exp}} \right)^2 .$$

In this equation, the summation extends over all the experimental data points i that are considered for the fit, σ_i^{exp} is the estimated uncertainty of the measured peak intensity I_i^{exp}, $I_i^{calc}(\xi)$ is the calculated peak intensity and $\xi = (x_1, \ldots, x_n)$ is the set of adjustable model parameters. Uncertainties in measured intensities, σ_i^{exp}, were estimated based on the apparent intensity scatter present in the baseline of the CEST profiles. Intensities, $I_i^{calc}(\xi)$, were calculated by numerical integration of the Bloch-McConnell equations [65] (over the interval T_{CEST}) describing the

evolution of a single ^{13}C spin. Weak scalar coupling to one, two or three additional ^{13}C spins (depending on the number of directly coupled nuclei for the carbon under consideration) is included, as described below. The spin in turn exchanges between two states, *G* and *E*, with rates k_{GE} and k_{EG}. The appropriate equations are given elsewhere [34,35]. The x, y and z components of magnetization were calculated for both the *G* and *E* states, for each spectral line of the multiplet arising from the different combinations of spin "up" and "down" of the adjacent, coupled ^{13}C spins. $^{1}J_{CC}$ values of 35 Hz and 51 Hz were used for aliphatic–aliphatic and aliphatic–carbonyl or aliphatic–aromatic ^{13}C–^{13}C couplings, respectively [66]. Each multiplet component is assumed to relax identically, and cross-relaxation between individual lines within a multiplet and between adjacent ^{13}C spins is neglected. In this way, each line of a multiplet can be treated using the same formalism as for an isolated spin, with identical longitudinal (R_1) and transverse (R_2) relaxation rates for each component. Parameters included in the fit were k_{ex} ($k_{GE} + k_{EG}$), p_E (the fractional population of state *E*), $\Delta\varpi_{GE} = \varpi_E - \varpi_G$ (^{13}C chemical shift difference between states *G* and *E*; ppm), R_1, R_2 and an initial intensity (I_0). Note that both longitudinal (R_1) and transverse (R_2) relaxation rates were assumed to be identical in states *G* and *E*. Although the experiment is sensitive to the linewidth (R_2) of each state, no significant, statistical improvements in the quality of the fits were observed when adding an extra fitting parameter (per residue) to account for linewidth differences between *G* and *E* states (a strong indication that corresponding nuclei for both states have similar intrinsic transverse relaxation rates). It should be noted that k_{ex} and p_E were global parameters, while $\Delta\varpi_{GE}$, R_1 and R_2 were fit individually for each ^{13}C spin and I_0 was fit for each ^{13}C–^{1}H pair. ^{13}C chemical shift values of the ground state were extracted from a separate correlation map (see above) and were fixed in the fits.

^{15}N CEST experiments were fit in a similar manner, taking into account couplings with surrounding carbons [67] ($^{1}J_{NCO} = -14.4$ Hz, $^{1}J_{NC\alpha} = -10.7$ Hz and $^{2}J_{NC\alpha} = -7.7$ Hz). Practically, a subset of ^{15}N CEST profiles derived from residues with $|\Delta\varpi_{GE}| > 2.0$ ppm was globally fit in order to obtain accurate p_E and k_{ex} values. Resulting k_{ex} and p_E values were then used as fixed parameters in the fit of ^{13}C CEST profiles.

Data deposition

^{13}C chemical shifts of the excited states of the G48A Fyn SH3 and L24A FF domains have been deposited with the BMRB (accession numbers 19590 and 19591, respectively).

Acknowledgements

The authors are grateful to Dr. Mark V. Berjanskii (University of Alberta) for useful discussions on RCI_{SC} and for providing a version of his program optimized for side-chain ^{13}C chemical shifts exclusively. The work was supported by grants from the Natural Sciences and Engineering Research Council of Canada and the Canadian Institutes of Health Research. L.E.K. holds a Canada Research Chair in Biochemistry.

Appendix A. Supplementary data

Supplementary data to this article can be found online at http://dx.doi.org/10.1016/j.jmb.2013.10.041.

Received 24 October 2013;
Received in revised form 31 October 2013;
Accepted 31 October 2013
Available online 8 November 2013

Keywords:
CEST;
conformationally excited states;
chemical shifts;
protein side chains

Abbreviations used:
CEST, chemical exchange saturation transfer; CPMG, Carr–Purcell–Meiboom–Gill; 2D, two-dimensional; BMRB, Biological Magnetic Resonance Bank; FID, free induction decay.

References

[1] Karplus M, Kuriyan J. Molecular dynamics and protein function. Proc Natl Acad Sci USA 2005;102:6679–85.
[2] Nikolova EN, Kim E, Wise AA, O'Brien PJ, Andricioaei I, Al-Hashimi HM. Transient Hoogsteen base pairs in canonical duplex DNA. Nature 2011;470:498–502.
[3] Korzhnev DM, Salvatella X, Vendruscolo M, Di Nardo AA, Davidson AR, Dobson CM, et al. Low-populated folding intermediates of Fyn SH3 characterized by relaxation dispersion NMR. Nature 2004;430:586–90.
[4] Chiti F, Dobson CM. Amyloid formation by globular proteins under native conditions. Nat Chem Biol 2009;5:15–22.
[5] McParland VJ, Kalverda AP, Homans SW, Radford SE. Structural properties of an amyloid precursor of beta(2)-microglobulin. Nat Struct Biol 2002;9:326–31.
[6] Neudecker P, Robustelli P, Cavalli A, Walsh P, Lundstrom P, Zarrine-Afsar A, et al. Structure of an intermediate state in protein folding and aggregation. Science 2012;336:362–6.
[7] Sugase K, Dyson HJ, Wright PE. Mechanism of coupled folding and binding of an intrinsically disordered protein. Nature 2007;447:1021–4.
[8] Tang C, Iwahara J, Clore GM. Visualization of transient encounter complexes in protein–protein association. Nature 2006;444:383–6.
[9] Boehr DD, McElheny D, Dyson HJ, Wright PE. The dynamic energy landscape of dihydrofolate reductase catalysis. Science 2006;313:1638–42.
[10] Fraser JS, Clarkson MW, Degnan SC, Erion R, Kern D, Alber T. Hidden alternative structures of proline isomerase essential for catalysis. Nature 2009;462:669–73.
[11] Ishima R, Freedberg DI, Wang YX, Louis JM, Torchia DA. Flap opening and dimer-interface flexibility in the free and

inhibitor-bound HIV protease, and their implications for function. Structure 1999;7:1047–55.
[12] Rivalta I, Sultan MM, Lee NS, Manley GA, Loria JP, Batista VS. Allosteric pathways in imidazole glycerol phosphate synthase. Proc Natl Acad Sci USA 2012;109:E1428–36.
[13] Dethoff EA, Chugh J, Mustoe AM, Al-Hashimi HM. Functional complexity and regulation through RNA dynamics. Nature 2012;482:322–30.
[14] Palmer AG, Kroenke CD, Loria JP. NMR methods for quantifying microsecond-to-millisecond motions in biological macromolecules. Methods Enzymol 2001;339:204–38.
[15] Ishima R, Torchia DA. Protein dynamics from NMR. Nat Struct Biol 2000;7:740–3.
[16] Mittermaier A, Kay LE. New tools provide new insights in NMR studies of protein dynamics. Science 2006;312:224–8.
[17] Korzhnev DM, Religa TL, Banachewicz W, Fersht AR, Kay LE. A transient and low-populated protein-folding intermediate at atomic resolution. Science 2010;329:1312–6.
[18] Vallurupalli P, Hansen DF, Kay LE. Structures of invisible, excited protein states by relaxation dispersion NMR spectroscopy. Proc Natl Acad Sci USA 2008;105:11766–71.
[19] Bouvignies G, Vallurupalli P, Hansen DF, Correia BE, Lange O, Bah A, et al. Solution structure of a minor and transiently formed state of a T4 lysozyme mutant. Nature 2011;477:111–4.
[20] Hansen DF, Vallurupalli P, Kay LE. Using relaxation dispersion NMR spectroscopy to determine structures of excited, invisible protein states. J Biomol NMR 2008;41:113–20.
[21] Lundstrom P, Teilum K, Carstensen T, Bezsonova I, Wiesner S, Hansen DF, et al. Fractional ^{13}C enrichment of isolated carbons using [1-^{13}C]- or [2-^{13}C]-glucose facilitates the accurate measurement of dynamics at backbone Calpha and side-chain methyl positions in proteins. J Biomol NMR 2007;38:199–212.
[22] Lundstrom P, Hansen DF, Vallurupalli P, Kay LE. Accurate measurement of alpha proton chemical shifts of excited protein states by relaxation dispersion NMR spectroscopy. J Am Chem Soc 2009;131:1915–26.
[23] Goto NK, Gardner KH, Mueller GA, Willis RC, Kay LE. A robust and cost-effective method for the production of Val, Leu, Ile (δ1) methyl-protonated ^{15}N-,^{13}C-,^{2}H-labeled proteins. J Biomol NMR 1999;13:369–74.
[24] Korzhnev DM, Kloiber K, Kanelis V, Tugarinov V, Kay LE. Probing slow dynamics in high molecular weight proteins by methyl-TROSY NMR spectroscopy: application to a 723-residue enzyme. J Am Chem Soc 2004;126:3964–73.
[25] Janin J, Miller S, Chothia C. Surface, subunit interfaces and interior of oligomeric proteins. J Mol Biol 1988;204:155–64.
[26] Lundstrom P, Kay LE. Measuring 13Cb chemical shifts of invisible excited states in proteins by relaxation dispersion NMR spectroscopy. J Biomol NMR 2009;44:139–55.
[27] LeMaster DM, Kushlan DM. Dynamical mapping of *E. coli* thioredoxin via ^{13}C NMR relaxation analysis. J Am Chem Soc 1996;118:9255–64.
[28] Ishima R, Baber J, Louis JM, Torchia DA. Carbonyl carbon transverse relaxation dispersion measurements and ms-micros timescale motion in a protein hydrogen bond network. J Biomol NMR 2004;29:187–98.
[29] Forsen S, Hoffman RA. Study of moderately rapid chemical exchange reactions by means of nuclear magnetic double resonance. J Chem Phys 1963;39:2892–901.
[30] Gupta RK, Redfield AG. Double nuclear magnetic resonance observation of electron exchange between ferri- and ferrocytochrome c. Science 1970;169:1204–6.
[31] Cayley PJ, Albrand JP, Feeney J, Roberts GC, Piper EA, Burgen AS. Nuclear magnetic resonance studies of the binding of trimethoprim to dihydrofolate reductase. Biochemistry 1979;18:3886–95.
[32] Ward KM, Aletras AH, Balaban RS. A new class of contrast agents for MRI based on proton chemical exchange dependent saturation transfer (CEST). J Magn Reson 2000;143:79–87.
[33] Zhou JY, van Zijl PCM. Chemical exchange saturation transfer imaging and spectroscopy. Prog Nucl Magn Reson Spectrosc 2006;48:109–36.
[34] Fawzi NL, Ying J, Ghirlando R, Torchia DA, Clore GM. Atomic-resolution dynamics on the surface of amyloid-beta protofibrils probed by solution NMR. Nature 2011;480:268–72.
[35] Vallurupalli P, Bouvignies G, Kay LE. Studying "invisible" excited protein states in slow exchange with a major conformation. J Am Chem Soc 2012;134:8148–61.
[36] Bouvignies G, Kay LE. A 2D (1)(3)C-CEST experiment for studying slowly exchanging protein systems using methyl probes: an application to protein folding. J Biomol NMR 2012;53:303–10.
[37] Vallurupalli P, Kay LE. Probing slow chemical exchange at carbonyl sites in proteins by chemical exchange saturation transfer NMR spectroscopy. Angew Chem Int Ed Engl 2013;52:4156–9.
[38] Hansen AL, Bouvignies G, Kay LE. Probing slowly exchanging protein systems via (13)C (alpha)-CEST: monitoring folding of the Im7 protein. J Biomol NMR 2013;55:279–89.
[39] Bouvignies G, Kay LE. Measurement of proton chemical shifts in invisible states of slowly exchanging protein systems by chemical exchange saturation transfer. J Phys Chem B 2012;116:14311–7.
[40] Vallurupalli P, Bouvignies G, Kay LE. A computational study of the effects of ^{13}C–^{13}C scalar couplings on ^{13}C CEST NMR spectra: towards studies on a uniformly ^{13}C-labeled protein. ChemBioChem 2013;14:1709–13.
[41] Tollinger M, Skrynnikov NR, Mulder FAA, Forman-Kay JD, Kay LE. Slow dynamics in folded and unfolded states of an SH3 domain. J Am Chem Soc 2001;123:11341–52.
[42] Ernst RR, Bodenhausen G, Wokaun A. Principles of nuclear magnetic resonance in one and two dimensions. Oxford: Oxford University Press; 1987.
[43] Pawson T. Protein modules and signalling networks. Nature 1995;373:573–80.
[44] Di Nardo AA, Korzhnev DM, Stogios PJ, Zarrine-Afsar A, Kay LE, Davidson AR. Dramatic acceleration of protein folding by stabilization of a nonnative backbone conformation. Proc Natl Acad Sci USA 2004;101:7954–9.
[45] Press WH, Flannery BP, Teukolsky SA, Vetterling WT. Numerical recipes in C. Cambridge: Cambridge University Press; 1988.
[46] Tamiola K, Acar B, Mulder FA. Sequence-specific random coil chemical shifts of intrinsically disordered proteins. J Am Chem Soc 2010;132:18000–3.
[47] Wishart DS, Bigam CG, Holm A, Hodges RS, Sykes BD. ^{1}H, ^{13}C and ^{15}N random coil NMR chemical shifts of the common amino acids. I. Investigations of nearest-neighbor effects. J Biomol NMR 1995;5:67–81.
[48] Korzhnev DM, Vernon RM, Religa TL, Hansen AL, Baker D, Fersht AR, et al. Nonnative interactions in the FF domain folding pathway from an atomic resolution structure of a sparsely populated intermediate: an NMR relaxation dispersion study. J Am Chem Soc 2011;133:10974–82.

[49] Berjanskii MV, Wishart DS. A simple method to predict protein flexibility using secondary chemical shifts. J Am Chem Soc 2005;127:14970–1.
[50] Jemth P, Gianni S, Day R, Li B, Johnson CM, Daggett V, et al. Demonstration of a low-energy on-pathway intermediate in a fast-folding protein by kinetics, protein engineering, and simulation. Proc Natl Acad Sci USA 2004;101:6450–5.
[51] Korzhnev DM, Religa TL, Lundstrom P, Fersht AR, Kay LE. The folding pathway of an FF domain: characterization of an on-pathway intermediate state under folding conditions by (15)N, (13)C(alpha) and (13)C-methyl relaxation dispersion and (1)H/(2)H-exchange NMR spectroscopy. J Mol Biol 2007;372:497–512.
[52] McCully ME, Beck DA, Fersht AR, Daggett V. Refolding the engrailed homeodomain: structural basis for the accumulation of a folding intermediate. Biophys J 2010;99:1628–36.
[53] Wensley BG, Batey S, Bone FA, Chan ZM, Tumelty NR, Steward A, et al. Experimental evidence for a frustrated energy landscape in a three-helix-bundle protein family. Nature 2010;463:685–8.
[54] Feng H, Zhou Z, Bai Y. A protein folding pathway with multiple folding intermediates at atomic resolution. Proc Natl Acad Sci USA 2005;102:5026–31.
[55] Capaldi AP, Kleanthous C, Radford SE. Im7 folding mechanism: misfolding on a path to the native state. Nat Struct Biol 2002;9:209–16.
[56] Berjanskii MV, Wishart DS. A simple method to measure protein side-chain mobility using NMR chemical shifts. J Am Chem Soc 2013;135:14536–9.
[57] Ruschak AM, Religa TL, Breuer S, Witt S, Kay LE. The proteasome antechamber maintains substrates in an unfolded state. Nature 2010;467:868–71.
[58] Jemth P, Day R, Gianni S, Khan F, Allen M, Daggett V, et al. The structure of the major transition state for folding of an FF domain from experiment and simulation. J Mol Biol 2005;350:363–78.
[59] Sattler M, Schleucher J, Griesinger C. Heteronuclear multidimensional NMR experiments for the structure determination of proteins in solution employing pulsed field gradients. Prog Nucl Magn Reson Spectrosc 1999;34:93–158.
[60] Guenneugues M, Berthault P, Desvaux H. A method for determining B1 field inhomogeneity. Are the biases assumed in heteronuclear relaxation experiments usually underestimated? J Magn Reson 1999;136:118–26.
[61] Abragam A. Principles of nuclear magnetism. Oxford: Clarendon Press; 1961.
[62] Delaglio F, Grzesiek S, Vuister GW, Zhu G, Pfeifer J, Bax A. NMRPipe: a multidimensional spectral processing system based on UNIX pipes. J Biomol NMR 1995;6:277–93.
[63] Kneller D, Kuntz I. UCSF Sparky—an NMR display, annotation and assignment tool. J Cell Biochem 1993;17C:254.
[64] Vranken WF, Boucher W, Stevens TJ, Fogh RH, Pajon A, Llinas M, et al. The CCPN data model for NMR spectroscopy: development of a software pipeline. Proteins 2005;59:687–96.
[65] McConnell HM. Reaction rates by nuclear magnetic resonance. J Chem Phys 1958;28:430–1.
[66] Bystrov VF. Spin-spin coupling and the conformational states of peptide systems. Prog NMR Spectrosc 1976;10:41–81.
[67] Cavanagh J, Fairbrother WJ, Palmer AG, Skelton NJ. Protein NMR spectroscopy: principles and practice. San Diego: Academic Press; 1996.